Impact of nonlinear hydrodynamic modelling on geometric optimisation of a spherical heaving point absorber

Bingyong Guo, Qusai Elmoosa, Christian Windt, John V. Ringwood

Abstract—**Due to the amount of iterative computation involved, researchers involved in geometric optimisation of wave energy devices typically employ linear hydrodynamic models. However, the exaggerated motion of wave energy devices, aided by energy maximising control action, challenges the assumptions upon which linear hydrodynamic modelling relies. Furthermore, the optimal device geometry is also sensitive to the nature of the energy-maximisation controller employed, and to the set of wave conditions over which the optimisation is carried out.**

In order to focus on the essential issues, this study takes the simplest possible device for optimisation, a heaving sphere (with just one free parameter), but one which exhibits nonlinear hydrodynamic characteristics, due to the non-uniform cross-sectional area. The study examines the sensitivity to the inclusion of nonlinear Froude-Krylov forces. In addition, the sensitivity of the optimal device size to differences in the applied control algorithm is also studied, as are effects due to different representative sea state representations and performance evaluation criteria.

Index Terms—**wave energy converter, geometric optimisation, wave energy control, hydrodynamic modelling, sensitivity**

I. Introduction

WAVE energy is one of the few untapped sources of renewable energy that could make a significant contribution to the future energy system. Unfortunately, to date, no wave energy converters (WECs) have proven themselves to be commercially viable for the utility market. One of the reasons for this is the diversity in design directions, due to the many wave energy conversion principles upon which WECs are based and the wide variety of WEC geometric shapes used to harness energy based on those principles.

In general, the development of a WEC project is costly, time-consuming, and high-risk [1], [2]. Conventional WEC development focuses on advancing technology readiness levels (TRLs) from 1 to 9, and the corresponding development cost and time are up to 50 M€ and 10 years [1], [2], respectively, resulting in a high levelised cost of energy (LCoE). By summarising existing WEC projects, it is recommended to evaluate technology performance levels (TPLs), even at low TRLs, to save development time and cost, and to mitigate development risk [1]–[5]. For a generic WEC device, design optimisation, especially geometric optimisation and optimal control, is required at early stages ofthe WEC development [1], [4], [5], to improve techno-economic performance [6]–[8].

A generic WEC geometric optimisation procedure is illustrated in Fig. 1. For an initial WEC device concept, the first step is to define the WEC geometry and its operational mode(s) according to the sea states of the deployment site, to harvest wave energy via wave-structure interaction (WSI). In general, control strategies are applied to the WSI model, in order to exaggerate WEC motion and maximise power capture [9]. However, large WEC motion consequently leads to nonlinear hydrodynamic behaviour [9]. In addition, the WSI-based model, derived from hydrodynamic modelling tools, e.g. boundary element methods (BEM) and computational fluid dynamics (CFD) packages, may be computationally expensive. Given the naturally high number of optimisation iterations, model simplification is required for applying control strategies, computing WEC dynamics and evaluating WEC performance. Finally, optimisation algorithms are used to update the WEC geometry until performance is maximised.

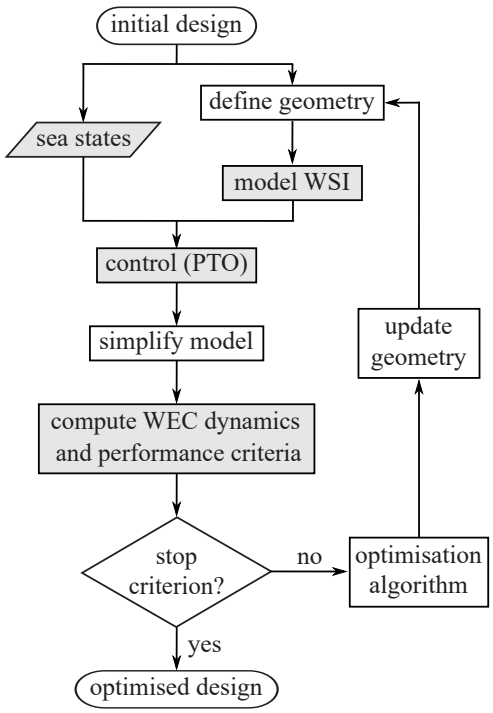

Fig. 1. Geometric optimisation flowchart of a wave energy converter.

B. Guo and J.V. Ringwood are with Centre for Ocean Energy Research, Maynooth University, Ireland (e-mail: bingyong.guo@mu.ie,john.ringwood@mu.ie; Qusai Elmoosa is with Hochschule Nordhausen (email: qusai.elmoosa@hs-nordhausen.de), Germany; Christian Windt is with Technische Universität Braunschweig, Germany (email: c.windt@tu-braunschweig.de).

As shown in Fig. 1, the sea states, geometry definition, WSI modelling, control, performance measures, and optimisation algorithms can all influence the optimised WEC geometry. The optimised hull, shape and dimensions are sensitive to WEC working principles [10], [11], sea states [12]–[15], control strategies [9], [16], [17] and performance criteria [6], [18]–[20]. In addition, the optimised result is also influenced by the geometry definition methods [21], [22] and optimisation algorithms [23]–[25]. The choice of optimisation algorithm mainly determines the computation time and likelihood of converging to global optimum [20].

For WEC geometric optimisation, most studies apply linear WSI modelling methods, either in the time [16], [26] or frequency domain [6], [27], [28]. Linear WSI modelling methods are computationally efficient, even in regular waves, but may be low in modelling fidelity, especially when the WEC is tuned to be resonant with the incident waves by power maximising control [9]. On the contrary, high-fidelity WSI methods, e.g. CFD, are computationally heavy [29]–[33], and may be not suitable for some WEC geometric optimisation, e.g. optimising the annual energy production of a device. Ultimately, for optimisation applications, a plausible balance between computational complexity and fidelity must be struck, with the availability of limited computing power. A trade-off between modelling fidelity and computing efficiency can be compromised by hybrid modelling methods, as summarised in [34].

Since a hydrodynamic model plays a crucial role in WEC geometry optimisation, it is to be expected that WSI modelling methods should have a significant influence on optimised geometry. However, there are few studies aiming to compare various WSI modelling methods in WEC geometric optimisation [35]. Meanwhile, WSI modelling fidelity is sensitive to sea states and control, and has a significant influence on WEC performance. Thus, the interplay between sea states, WSI modelling methods, control strategies, and performance criteria should be addressed in the WEC optimisation loop (see Fig. 1). This study uses the simplest WEC geometry, a semi-submerged sphere in heave, to examine the sensitivity of the optimal geometry to the nature of the hydrodynamic models employed. Linear and nonlinear hydrodynamic modelling methods are compared, with the former applying linear potential flow theory and the latter including nonlinear Froude-Krylov (FK) and hydrostatic forces (termed *weakly* nonlinear WSI method in this paper), with respect to instantaneous wetted surface. As WSI modelling methods are inherently coupled with sea states, control and performance measures (the shadowed blocks in Fig. 1), this study also examines the interplay of those factors. In addition, the parametric evaluation, over a defined parametric space, rather than a specific optimisation line search, is applied in this study, to evaluate the overall WEC performance against various criteria.

The remainder of the paper is organised as follows: Section II presents the various sea states employed for optimisation, while Section III describes the linear and weakly nonlinear hydrodynamic modelling methods. Section IV summarises the reactive and passive control strategies, with various performance criteria introduced in Section V. Numerical results are presented and discussed in Section VI. Finally, Section VII draws some conclusions and indicated potential future work.

II. Sea states

To optimise the geometry of a WEC system for a given installation site, long-term, e.g. annual or decadal, wave observation data are required to specify the wave climate. In this study, the data collected in 2017 at the Atlantic Marine Energy Test Site (AMETS) by the Belmullet Inner (Berth B) wave buoy [36] is used, which is shown in Fig. 2(a) in terms of the significant wave height H_s and the energy period T_e. The depth at the installation site of the Belmullet Inner wave buoy is about 50 m. In Fig. 2(a), the colour-bar represents the occurrence of each sea state in hours, and the data availability is up to 8723 hours out of 8760 hours, that is 99.58%.

Based on long-term wave data, an optimised WEC geometry can balance WEC performance across all the sea states presented in the optimisation framework. Some performance measures, such as annual energy production and capacity factor, can only be evaluated based on long-term wave observation. Thus, the geometric optimisation procedure is time-consuming, and computationally costly. One possible way to accelerate the optimisation is to use some characteristic sea states, e.g. the most energetic, frequent or/and average sea states in Fig. 2(b), as the simplified design wave conditions of the deployment site.

In general, sea states can be statistically represented by wave spectra, among which the notable ones are the joint North Sea wave project (JONSWAP) [37] and the Pierson-Moskowitz (PM) [38] spectral models. The JONSWAP spectrum, defined by significant wave height H_s and peak period T_p, is applied in this study, given as

$$S(\omega) = \alpha \frac{5H_\mathrm{s}^2}{16} \frac{\omega_\mathrm{p}^4}{\omega^5} \exp\left(-\frac{5\omega_\mathrm{p}^4}{4\omega^4}\right) \gamma^{\exp\left(-\frac{(\omega-\omega_\mathrm{p})^2}{2\delta^2\omega_\mathrm{p}^2}\right)}, \quad (1)$$

where $\omega_\mathrm{p} = \frac{2\pi}{T_\mathrm{p}}$ is the peak frequency. γ, α, and σ are the shape coefficients. In this study, $\gamma = 3.3$, $\alpha = 1 - 0.287 \ln \gamma$, $\delta = 0.07$ for $\omega \leq \omega_\mathrm{p}$ and $\delta = 0.09$ for $\omega \geq \omega_\mathrm{p}$ are applied. For $\gamma = 3.3$, $T_\mathrm{p} \approx 1.12 T_\mathrm{e}$ holds [39]. For a given sea state, the wave power flux per wave front is written as

$$J = \frac{\rho g^2}{64\pi} T_\mathrm{e} H_\mathrm{s}^2, \quad (2)$$

where ρ and g are the water density and gravitational acceleration constant, respectively.

Ocean waves are typically random and irregular, and can be approximated by the summation of a group of sinusoidal waves, given as

$$\eta(t) = \sum_{i=1}^{N} a_i \cos(\omega_i t + \varphi_i), \quad (3)$$

where a_i, ω_i and φ_i are the amplitude, frequency, and initial phase of the ith sinusoidal wave of N components, respectively. For a given wave spectrum,

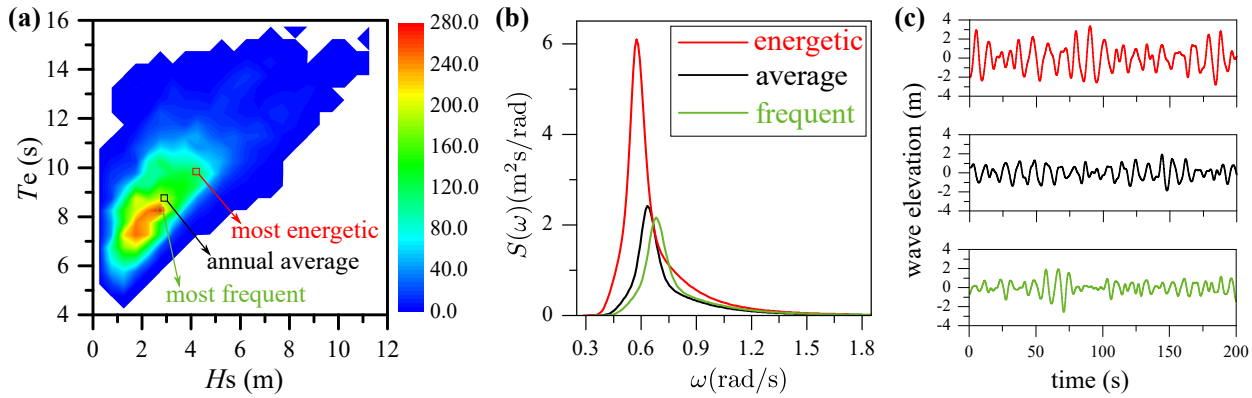

Fig. 2. (a) Wave climate at the Atlantic Marine Energy Test Site, (b) wave spectra and (c) time traces of wave elevation. In (a), the colorbar indicates the occurrence of sea states in hour.

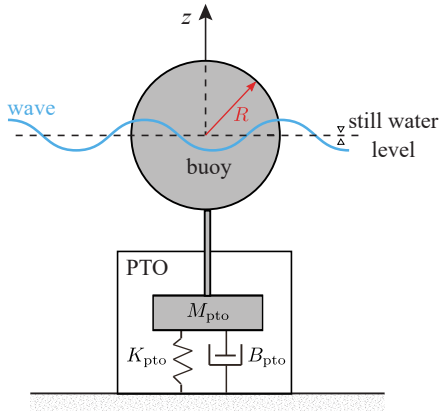

Fig. 3. A semi-submerged spherical point absorber in heave.

wave elevation in the time domain can be realised by randomising wave amplitudes or phases [40], of which the scheme of random phases and deterministic amplitudes is used to generate wave time traces, as shown in Fig. 2(c).

In this study, three characteristic sea states are used for geometric optimisation, including (i) the most energetic sea state with $H_{\rm s} = 4.25$ m and $T_{\rm e} = 9.75$ s, (ii) the annual average sea state with $H_{\rm s} = 2.81$ m and $T_{\rm e} = 8.84$ s, and (iii) the most frequent sea state with $H_{\rm s} = 2.75$ m and $T_{\rm e} = 8.25$ s. The wave spectra and corresponding time traces of those three sea states are illustrated in Figs. 2(b)-(c). As the depth at the installation site of the Belmullet Inner wave buoy is about 50 m, the deep water assumption is satisfied for the aforementioned sea states.

III. Hydrodynamic Modelling

The simplest WEC geometry, a semi-submerged heaving sphere, is shown in Fig. 3, and its motion is governed by Newton's second law, given as

$$M\ddot{z}_{\rm b}(t) = f_{\rm h}(t) + f_{\rm g}(t) + f_{\rm pto}(t), \tag{4}$$

where M, $\ddot{z}_{\rm b}$, and $z_{\rm b}$ are the sphere mass, heave acceleration, and displacement, respectively. $f_{\rm h}$, $f_{\rm g}$, and $f_{\rm pto}$ are the hydrodynamic, gravitational, and power take-off (PTO) forces, respectively.

The gravitational and PTO forces can be written as

$$f_{\rm g}(t) = -Mg, \tag{5}$$

$$f_{\rm pto}(t) = -M_{\rm pto}\ddot{z}_{\rm b}(t) - B_{\rm pto}\dot{z}_{\rm b}(t) - K_{\rm pto}z_{\rm b}(t), \tag{6}$$

where $M_{\rm pto}$, $B_{\rm pto}$, and $K_{\rm pto}$ are the PTO mass, damping, and stiffness, respectively. $\dot{z}_{\rm b}$ is the buoy velocity.

The hydrodynamic force can be expressed as the integral of the pressure p on the wetted surface S, as

$$f_{\rm h}(t) = -\iint_S p\boldsymbol{n}\ {\rm d}S, \tag{7}$$

where $\boldsymbol{n}$ is the normal vector on the wetted surface. Thus, the key to WSI modelling is to compute the distribution of the pressure p in the fluid. In general, the WEC hydrodynamics are governed by the Navier-Stokes equations and can be numerically computed, mainly via CFD software packages [29]. As optimisation (or parametric study) is naturally characterised by a high iteration count, linear potential flow (LPF) theory is widely used in the literature, and is applied in this study as one of the modelling approaches. To reveal the impact of WSI modelling methods on WEC optimisation, a weakly nonlinear hydrodynamics modelling method, using the instantaneous wetted surface to compute nonlinear FK and hydrostatic forces, is also applied, for comparison. Both modelling methods are detailed in the following two subsections.

A. Linear hydrodynamic modelling

Based on the assumptions of (i) an ideal fluid, i.e. incompressible, inviscid, and irrotational, (ii) small wave height, and (iii) small body motion, LPF theory can be applied to compute the pressure distribution in the fluid, which can be expressed as a function of the velocity potential function ϕ, given as

$$p = -\rho g z - \rho\frac{\partial\phi}{\partial t}, \tag{8}$$

where $p_{\rm s} = -\rho g z$ and $p_{\rm d} = -\rho\frac{\partial\phi}{\partial t}$ are the static and dynamic pressure, respectively. Based on the LPF theory, the total potential function can be divided into the incident, diffracted and radiated components, as

$$\phi = \phi_{\rm i} + \phi_{\rm d} + \phi_{\rm r}, \tag{9}$$

where $\phi_{\rm i}$, $\phi_{\rm d}$, and $\phi_{\rm r}$ are the potential functions associated with incident, diffracted, and radiated waves, respectively.

By assuming small wave height and the body motion, the wetted surface can be ideally treated as a constant. Thus, the hydrodynamic force can be approximately computed according to the wetted surface at the

body's equilibrium point in still water. Consequently, the hydrodynamic force f_{h} can be divided into the FK force f_{FK}, diffraction force f_{d}, radiation force f_{r}, and buoyancy force f_{b}, given as

$$f_{\mathrm{h}}(t) = f_{\mathrm{FK}}(t) + f_{\mathrm{d}}(t) + f_{\mathrm{r}}(t) + f_{\mathrm{b}}(t), \tag{10}$$

$$f_{\mathrm{FK}}(t) = \rho \iint_S \frac{\partial \phi_{\mathrm{i}}}{\partial t} \boldsymbol{n} \, \mathrm{d}S, \tag{11}$$

$$f_{\mathrm{d}}(t) = \rho \iint_S \frac{\partial \phi_{\mathrm{d}}}{\partial t} \boldsymbol{n} \, \mathrm{d}S, \tag{12}$$

$$f_{\mathrm{r}}(t) = \rho \iint_S \frac{\partial \phi_{\mathrm{r}}}{\partial t} \boldsymbol{n} \, \mathrm{d}S, \tag{13}$$

$$f_{\mathrm{b}}(t) = \rho \iint_S g z \boldsymbol{n} \, \mathrm{d}S, \tag{14}$$

where S is the invariant wetted surface at the equilibrium point in still water. Thus, $f_{\mathrm{b}} + f_{\mathrm{g}} = 0$ holds for a WEC body at rest in still water. When the body oscillates, the buoyancy force cannot match with the gravitational force and the mismatch is represented by the hydrostatic force f_{hs}, which is proportional to the buoy's displacement, given as

$$f_{\mathrm{hs}}(t) = f_{\mathrm{b}}(t) + f_{\mathrm{g}}(t) = -K z_{\mathrm{b}}(t), \tag{15}$$

where $K = \rho g \pi R^2$ is the hydrostatic stiffness and R is the radius of the sphere. In the frequency domain, the hydrostatic force can be rewritten as

$$F_{\mathrm{hs}}(\omega) = -K Z_{\mathrm{b}}(\omega), \tag{16}$$

where $Z_{\mathrm{b}}(\omega)$ is the frequency domain representation of the heave displacement z_{b}.

Based on Cummins' equation [41], the radiation force, in the time-domain, is given as

$$f_{\mathrm{r}}(t) = -A_{\infty} \ddot{z}_{\mathrm{b}}(t) - k_{\mathrm{r}}(t) * \dot{z}_{\mathrm{b}}(t), \tag{17}$$

where A_{∞} is the added mass at infinite frequency, and k_{r} is the impulse response function (IRF) associated with the radiation force. Alternatively, the radiation force can also be expressed in the frequency domain, rewritten as

$$F_{\mathrm{r}}(\omega) = \left(\omega^2 A(\omega) - j\omega B(\omega)\right) Z_{\mathrm{b}}(\omega), \tag{18}$$

where $F_{\mathrm{r}}(\omega)$, $A(\omega)$, and $B(\omega)$ are the frequency-domain representations of the radiation force, added mass and radiation damping, respectively. The reciprocal relationship between Eqs. (17) and (18) was derived by Ogilvie [42].

The convolution term $k_{\mathrm{r}} * \dot{z}_{\mathrm{b}}$ is not computationally efficient in WEC geometric optimisation and can be approximated by a finite-order state-space model, which can be identified by time-domain methods [43], [44] or frequency-domain methods [45]–[47]. As the moment-matching method in [46], [47] can guarantee the stability and passivity of the identified system, it is used in this study.

Based on LPF theory, the excitation force is defined as the summation of the FK and diffraction forces, and can be expressed as

$$f_{\mathrm{e}}(t) = f_{\mathrm{FK}} + f_{\mathrm{d}} = k_{\mathrm{e}}(t) * \eta(t), \tag{19}$$

where $k_{\mathrm{e}}(t)$ is the excitation IRF related to its frequency response function (FRF) $K_{\mathrm{e}}(\omega)$, as

$$k_{\mathrm{e}}(t) = \frac{1}{2\pi} \int_{-\infty}^{\infty} K_{\mathrm{e}}(\omega) e^{j\omega t} d\omega. \tag{20}$$

Thus, the excitation force can also be determined by its FRF, given as

$$F_{\mathrm{e}}(\omega) = K_{\mathrm{e}}(\omega) \bar{\eta}(\omega), \tag{21}$$

where $\bar{\eta}(\omega)$ is the frequency-domain representation of the incident wave $\eta(t)$.

It is well known that the excitation IRF, $k_{\mathrm{e}}(t)$, is non-causal and, thus, the convolution term in Eq. (19) cannot be parametrised directly. Extra efforts, e.g. wave prediction or up-stream wave measurement, are required to causalise the wave-to-excitation-force process. Several methods are proposed for approximating or estimating the excitation force, for example [48]–[51]. In this study, it is assumed that wave prediction is available and the method in [49], [50] is applied to model the excitation force from the incident waves. It is worth noting that the FK and diffraction forces in Eqs. (11)-(12) can be parametrised by the same procedure as employed with excitation force identification.

Substituting Eqs. (15)-(21) into Eq. (4), the linear WEC model can be rewritten as Cummins' equation, in the time- or frequency-domains, respectively, as

$$\begin{aligned} &(M + A_{\infty}) \ddot{z}_{\mathrm{b}}(t) + k_{\mathrm{r}}(t) * \dot{z}_{\mathrm{b}}(t) + K z_{\mathrm{b}}(t) \\ =& f_{\mathrm{e}}(t) + f_{\mathrm{pto}}(t), \end{aligned} \tag{22}$$

$$\begin{aligned} &\left[-\omega^2 \left(M + A(\omega)\right) + j\omega B(\omega) + K\right] Z_{\mathrm{b}}(\omega) \\ =& F_{\mathrm{e}}(\omega) + F_{\mathrm{pto}}(\omega), \end{aligned} \tag{23}$$

where $F_{\mathrm{pto}}(\omega)$ is the frequency-domain representation of the PTO force.

B. Weakly nonlinear hydrodynamic modelling

As WEC systems generally operate in mild to moderate sea states, the assumptions of an ideal fluid and small wave height can be met, to some extent. However, body motion can be exaggerated by power maximising control, and thus can generate some important nonlinear effects in WSI hydrodynamics [9]. Several nonlinear hydrodynamic factors, e.g. quadratic potential terms, nonlinear FK, radiation, hydrostatic, and viscous forces, are compared in [9], [52], which address the importance of the nonlinear FK, hydrostatic, and viscous forces. Although the viscous drag force can be included to Cummins' equation by adding a quadratic drag term, according to the Morison equation [53], the drag coefficient varies with waves [54], [55], and cannot keep a consistent value in WEC geometric optimisation. Thus, the weakly nonlinear hydrodynamic modelling method in this study only considers the nonlinear FK and hydrostatic forces induced by instantaneous wetted surface.

An algebraic representation of the nonlinear FK force for heaving axisymmetric point absorbers is detailed in [56]. Thus, this paper only gives an overview of the

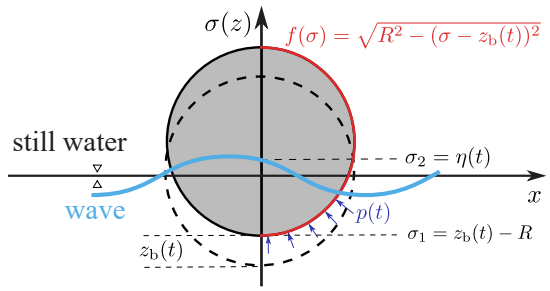

Fig. 4. An heaving point absorber with spherical profile.

nonlinear FK force modelling. Considering the time-varying wetted surface $S(t)$, the nonlinear FK and buoyancy forces can be rewritten as

$$f_{\mathrm{FK,nl}}(t) = \rho \iint_{S(t)} \frac{\partial \phi_{\mathrm{i}}}{\partial t} \boldsymbol{n} \, \mathrm{d}S, \tag{24}$$

$$f_{\mathrm{b,nl}}(t) = \rho \iint_{S(t)} g z \boldsymbol{n} \, \mathrm{d}S. \tag{25}$$

The nonlinear buoyancy force $f_{\mathrm{b,nl}}$ is also termed the nonlinear static FK force in [56]. For the heaving sphere in Fig. 4, the algebraic representations of $f_{\mathrm{FK,nl}}$ and $f_{\mathrm{b,nl}}$, derived in [56], are given as

$$f_{\mathrm{FK,nl}}(t) = \frac{2\pi}{k} \rho g \eta(t) \left[(z_{\mathrm{b}}(t) + \frac{1}{k} - \sigma) e^{k\sigma} \right]_{\sigma_1}^{\sigma_2}, \tag{26}$$

$$f_{\mathrm{b,nl}}(t) = -2\pi\rho g \left[-\frac{\sigma^3}{3} + z_{\mathrm{b}}(t) \frac{\sigma^2}{2} \right]_{\sigma_1}^{\sigma_2}, \tag{27}$$

where k is the wave number, σ is the the variable of integration, with integration limits of $\sigma_1 = z_{\mathrm{b}}(t) - R$ and $\sigma_2 = \eta(t)$.

Corresponding to the linear hydrostatic and excitation forces in Eqs. (15) and (19), respectively, the nonlinear 'hydrostatic force' and 'excitation force' can be defined as

$$f_{\mathrm{e,nl}}(t) = f_{\mathrm{FK,nl}}(t) + f_{\mathrm{d}}(t), \tag{28}$$

$$f_{\mathrm{hs,nl}}(t) = f_{\mathrm{b,nl}}(t) + f_{\mathrm{g}}(t). \tag{29}$$

Hence, the weakly nonlinear WEC model can be rewritten as

$$M \ddot{z}_{\mathrm{b}}(t) = f_{\mathrm{e,nl}}(t) + f_{\mathrm{r}}(t) + f_{\mathrm{hs,nl}}(t) + f_{\mathrm{pto}}(t). \tag{30}$$

For the weakly nonlinear modelling method applied in this study, the nonlinear FK force $f_{\mathrm{FK,nl}}$ and buoyancy force $f_{\mathrm{b,nl}}$ are computed according to Eqs. (26)-(27), while the diffraction force f_{d} and radiation force f_{r} are kept linear. It is worth noting that the algebraic presentations in Eqs. (26)-(27) assume that the WEC is a point absorber with an axisymmetric hull.

IV. Power Maximisation Control

The frequency-domain Cummins' equation in Eq. (23) can be rewritten as

$$\frac{V_{\mathrm{b}}(\omega)}{F_{\mathrm{e}}(\omega) + F_{\mathrm{pto}}(\omega)} = \frac{1}{Z_{\mathrm{i}}(\omega)}, \tag{31}$$

where $V_{\mathrm{b}}(\omega)$ is the frequency-domain expression of the body velocity $v_{\mathrm{b}}(t) = \dot{z}_{\mathrm{b}}(t)$. $Z_{\mathrm{i}}(\omega)$ is the intrinsic impedance of the system, defined as

$$Z_{\mathrm{i}}(\omega) = B(\omega) + j\omega \left[M + A(\omega) - \frac{K}{\omega^2} \right]. \tag{32}$$

According to the maximum power transfer theorem, the optimal PTO impedance should satisfy

$$Z_{\mathrm{pto}}(\omega) = B_{\mathrm{pto}}(\omega) + j\omega \left[M_{\mathrm{pto}} - \frac{K_{\mathrm{pto}}}{\omega^2} \right] = Z_{\mathrm{i}}^*(\omega). \tag{33}$$

Such a control law is called complex conjugate control or reactive control (RC) [57], which requires bi-directional power flow. If only uni-directional power flow is allowed, the PTO impedance reduces to a pure damper, resulting in so-called passive control (PC), given as

$$B_{\mathrm{pto}}(\omega) = |Z_{\mathrm{i}}(\omega)|. \tag{34}$$

Thus, the PTO force can be represented as $f_{\mathrm{pto}}(t) = -Z_{\mathrm{pto}} v_{\mathrm{b}}(t)$ for RC, or $f_{\mathrm{pto}}(t) = -B_{\mathrm{pto}} v_{\mathrm{b}}(t)$ for PC.

These classical control methods, i.e. RC and PC, are generally used in WEC geometric optimisation, as they usually give simple and computationally efficient forms for power maximising control. Although the RC and PC control strategies in Eqs. (33)-(34) are based on monochromatic waves, and they can be extended to irregular waves by selecting the parameters in Eqs. (33)-(34) according to some characteristic wave period metrics, e.g. peak, energy or zero-crossing periods, of a given wave spectrum [16], [58], [59]. In this study, the energy period is used to determine the PTO parameters.

V. Performance Criteria

Even though performance measures play a significant role in WEC geometric optimisation, there is no universal consensus on an appropriate (accessible) metric for WEC performance [4], [35]. Various performance criteria are used for WEC geometric optimisation, and can be classified as economic, technical and techno-economic criteria, which are introduced as follows.

As wave energy itself is free, the ultimate performance measure should be the LCoE over the lifetime of a WEC project, which can be defined by the present value (PV) approach [60], given as

$$\mathrm{LCoE} = \frac{\mathrm{PV(CapEx)} + \mathrm{PV(OpEx)}}{\mathrm{PV(AEP)}}, \tag{35}$$

where CapEx, OpEx, and AEP are capital expenditure, operation and maintenance expenditure, and annual energy production, respectively. Given that only limited operational experience of WEC projects is available [61], large uncertainties exist in LCoE estimation and modelling. In addition, a realistic LCoE model inherently contains a cluster of sub-models for WEC operational wave conditions, manufacturing, deployment, operation and maintenance, and productivity [60], which are, in general, computationally intractable for WEC shape optimisation.

Technical performance criteria are generally sensitive to device geometry, such as average absorbed power P_{a}, and capture width ratio (CWR). In general, the average absorbed power can be written as

$$P_{\mathrm{a}} = \frac{1}{T} \int_0^T f_{\mathrm{pto}}(t) \, v_{\mathrm{b}}(t) \, \mathrm{d}t, \tag{36}$$

where T is the time span, ranging from seconds to years. Historically, the hydrodynamic efficiency of a WEC device is mainly represented by the capture width ratio, given as

$$CWR = \frac{P_{\mathrm{a}}}{2JR}. \tag{37}$$

These two technical performance criteria are widely applied for WEC hull optimisation, even though they cannot reflect WEC economic performance [35].

By further assuming that $CapEx$ and $OpEx$ are proportional to some characteristic parameters of the WEC geometry, e.g. mean wetted area or displaced volume, the minimisation of LCoE is usually reduced to maximisation of some techno-economic performance criteria, such as average absorbed power per mean submerged area (P_{s}), or average absorbed power per displaced volume (P_{v}), which can be defined as

$$P_{\mathrm{s}} = \frac{P_{\mathrm{a}}}{A_{\mathrm{s}}}, \tag{38}$$

$$P_{\mathrm{v}} = \frac{P_{\mathrm{a}}}{V_{\mathrm{d}}}, \tag{39}$$

where A_{s} and V_{d} are the mean submerged area and the displaced volume, respectively. A preliminary study, based on a wave farm of CorPower devices with an installation capacity of 20 MW [7], shows clearly that LCoE is strongly related to more simplified techno-economic criteria, concluding that a maximum value of P_{s} generally achieves a low LCoE around its minimum value, and that a maximised P_{v} always results in a minimised LCoE.

In this study, the technical and techno-economic criteria in Eqs. (36)-(39) are investigated with various sea states, modelling methods and control strategies, in order to give an initial indication of their interrelationship, in the WEC geometric optimisation.

VI. Result and discussion

In this study, a simple WEC geometry, a semi-submerged heaving sphere, is used. The most energetic, annual average and most frequent sea stats described in Fig. 2 are applied as design wave conditions. Both the linear and weakly nonlinear hydrodynamic modelling methods in Section III are compared, with the linear WSI obtained from NEMOH (a BEM package). Both the RC and PC control philosophies in Eqs. (33)-(34) are extended to irregular waves by selecting the PTO impedance and resistance at the energy period of each sea state. The technical and techno-economic criteria in Eqs. (36)-(39) are evaluated. Full parametric analysis, rather than a line search, is used to illustrate the overall profile of the technical and techno-economic criteria in Eqs. (36)-(39), by varying the radius from 1 to 40 meters. For each iteration, the simulation time is 3000 seconds and the data of the last 2000 seconds are used to compute the performance criteria in Eqs. (36)-(39), as shown in Figs. 5-6.

The interplay between WSI modelling methods and sea state is illustrated in terms of the average power, using both PC and RC in Figs. 5(a) and (b), respectively. In general, the optimal power absorption and radius, achieved using the linear WSI modelling method, are lower or smaller than their weakly nonlinear WSI model counterparts, regardless of the particular control strategy or sea state employed. For the weakly nonlinear WSI model, the nonlinear FK and hydrostatic forces lead to a larger peak value of the excitation force (further illustrated in Fig. 7), and a smaller linear equivalent value of the hydrostatic stiffness, which contributes to a larger optimal radius. A more energetic sea state always results in a higher average power and a larger optimised radius, regardless of the WSI modelling method or control strategy employed. Compared to PC, RC can lead to a smaller radius, and the optimised radius is more robust to the variation in sea state and WSI modelling method. For PC, the device natural frequency should be designed around the prevailing wave frequency. As shown in Fig. 5, the prevailing wave frequency is low, resulting a large radius. On the contrary, optimal control strategies, e.g. RC, are capable to tune the device to be resonant with incident waves, showing a lower sensitivity to the device natural frequency and the prevailing wave frequency. Thus, the optimised radius is relatively sensitive to sea state and WSI modelling method, but optimal control has the capability to mitigate these sensitivities [58].

The interplay between WSI modelling methods and control strategies is demonstrated by evaluating various performance criteria, involving average power, capture width ratio, average power per wetted surface, and average power per displaced volume, shown in Figs. 6(a)-(b), respectively. In Fig. 6, the most frequent sea state is used as the design wave conditions. By evaluating the average power over a wide range of radius values, there always exists an optimum for each power curve in Fig. 6(a), regardless of the WSI modelling method or control strategy utilised. The CWR curves, for various modelling and control methods, are shown in Fig. 6(b), of which the CWR curves using RC monotonically decease as the radius increases, while there may exist multiple maxima in the CWR curves using PC. Thus, special care should be taken to find the global optima by selecting suitable (perhaps stochastic or concurrent) optimisation algorithms. In Figs. 6(c)-(d), both the average power per wetted surface, and the average power per displaced volume, decrease monotonically with increasing radius, regardless of the modelling and control approaches applied.

By parametrically evaluating and comparing various performance criteria over a wide range of radii, it can be concluded that the WEC geometric optimisation problem is non-trivial and implicit, and improper selection of either modelling method, control strategy, performance criterion, optimisation algorithm, or parameter space, may result in unrealistic optimal design. For example, the optimal radius of $R = 6$ m by using linear model and RC in Fig. 6(a) is unrealistic, as the relative buoy displacement with respect to wave elevation is larger than the radius, indicating the occurrence of overtopping phenomenon, and the need of advanced control strategy to limit the buoy motion [58]. In Fig. 6(b), a limited parameter space

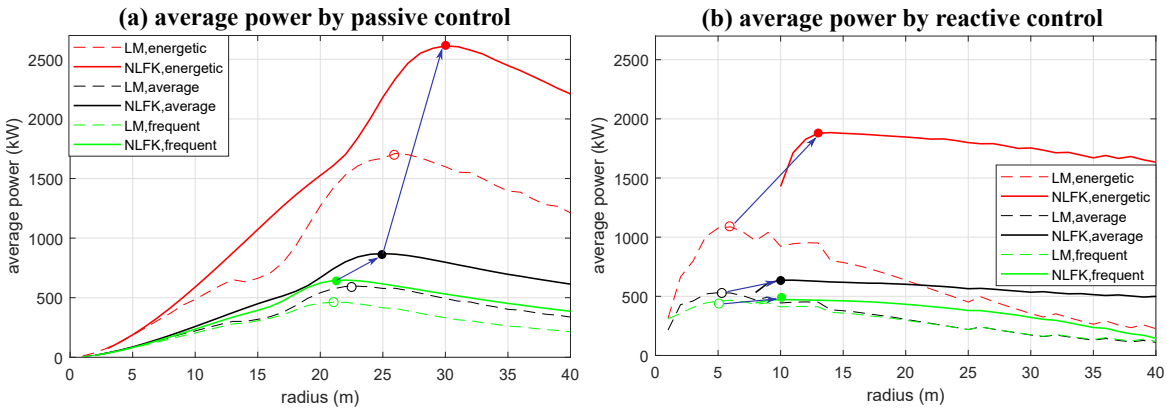

Fig. 5. Average absorbed power by (a) passive control and (b) reactive control, with various sea states. In the legend, LM means the linear model, NLFK means the weakly nonlinear model considering nonlinear FK force, and 'energetic', 'average', and 'frequent' indicate the most energetic, annual average, and most frequent sea states, respectively.

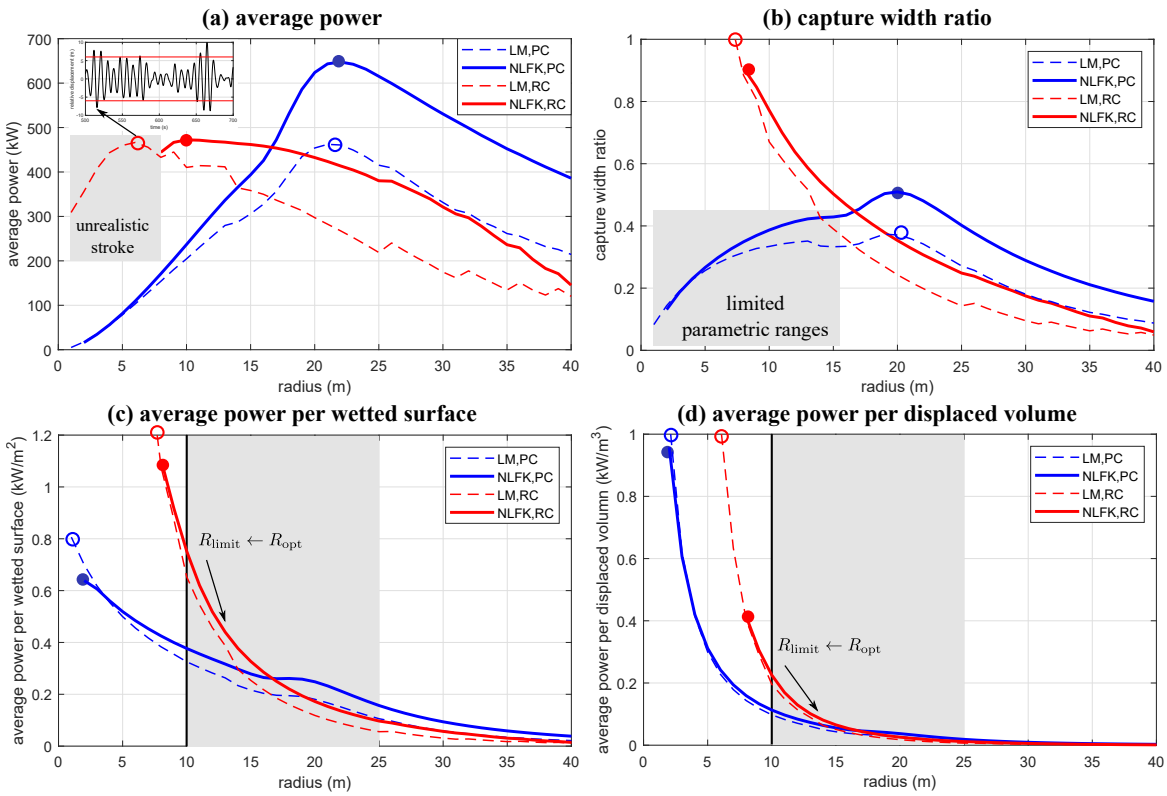

Fig. 6. Comparison of various performance criteria in the most frequent sea state with (a) average power, (b) capture width ratio, (c) average power per submerged area, and (d) average power per displaced volume. In the legend, LM, NLFK, PC and RC represent the linear model, weakly nonlinear model considering nonlinear FK force, passive control and reactive control, respectively.

or incongruous starting point may miss the global optima, especially when line search methods are used for multi-modal optimisation problem. For the average power per submerged area or per displaced volume, as shown in Figs. 6(c)-(d), respectively, the utility of conducting WEC geometric optimisation is doubtful, as the optimised radius always converges to the lower parametric limit, that is a shape of smallest volume.

To detail the effect of WSI modelling methods on WEC geometric optimisation, time traces for radii of 10 m and 20 m in the most frequency sea state are shown in Fig. 7, in terms of WEC displacement, hydrostatic force, excitation force, captured power and absorbed power. The captured power is defined as $f_{\text{e}}(t)v_{\text{b}}(t)$ for the linear model and as $f_{\text{e,nl}}(t)v_{\text{b}}(t)$ for the weakly nonlinear model, and the absorbed power is computed according to $f_{\text{pto}}(t)v_{\text{b}}(t)$.

For the case of $R = 10$ m, the WEC natural period is about 6.37 s, which is smaller than the energy period of the most frequent sea state ($T_{\text{e}} = 8.25$ s). That is, the prevailing wave frequency is lower than the WEC natural frequency. As shown in Fig. 7(a), the WEC displacement using RC is much larger than its counterpart using PC, leading to a larger restoring force in Fig. 7(b). In Fig. 7(c), the excitation force using RC only deviates slight from that using PC. Consequently, more power is captured and absorbed by using RC than PC, as shown in Figs. 7(d)-(e). On the other hand, the exaggerated WEC motion by RC causes a significant variation in the wetted surface, leading to a larger difference between linear and weakly nonlinear modelling methods. Compared to PC, RC can tune the WEC close to resonance, consequently resulting in larger oscillations, hydrostatic forces, with consequently higher captured

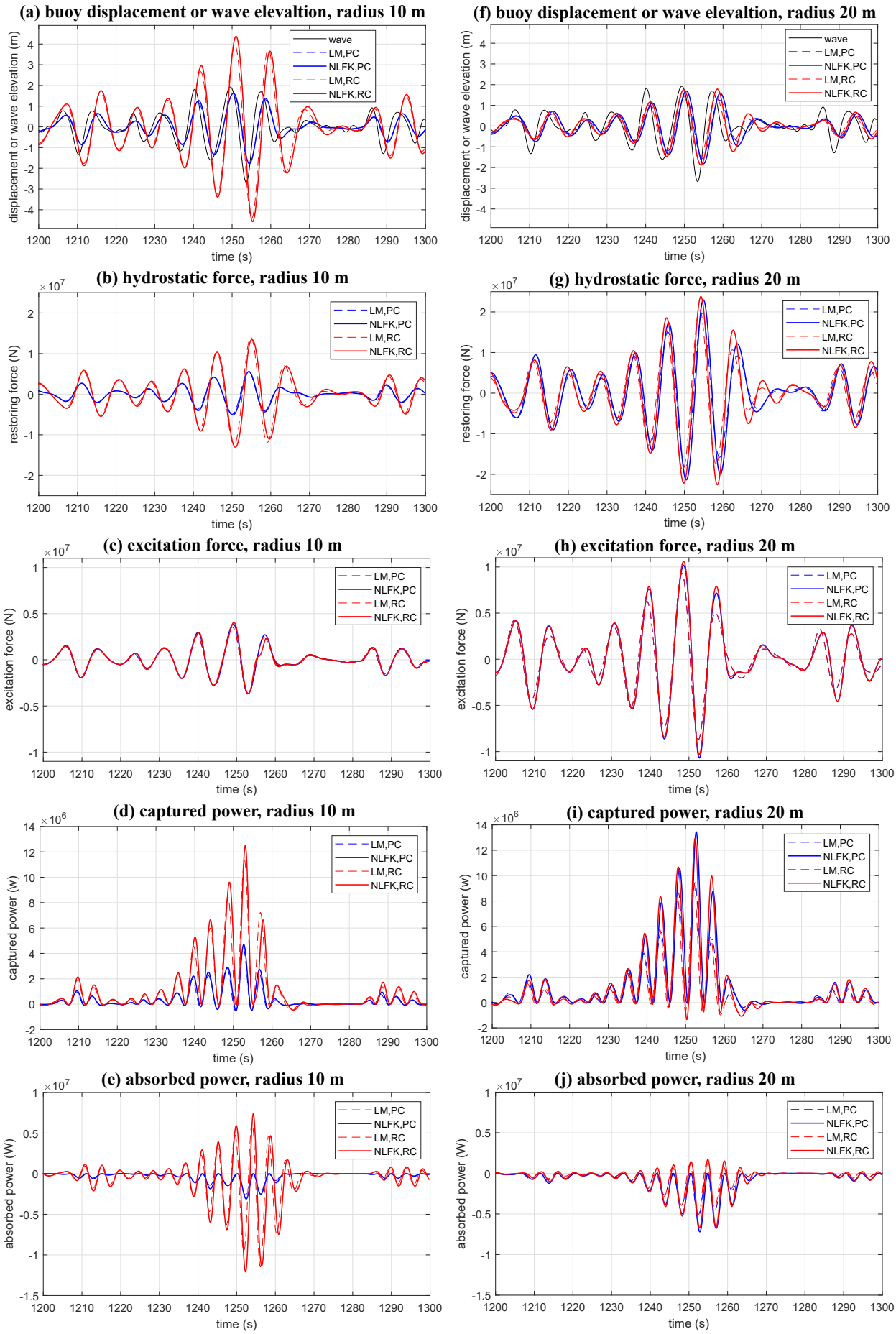

Fig. 7. Time traces for $R = 10$ m showing (a) WEC displacement, (b) hydrostatic force, (c) excitation force, (d) captured power, and (e) absorbed power, with their counterparts for $R = 20$ m in (f)-(j). In the legends, LM, NLFK, PC and RC represent the linear model, weakly nonlinear model considering nonlinear FK force, passive control and reactive control, respectively. The captured power in (d) and (i) is defined as $P_{\mathrm{e}}(t) = f_{\mathrm{e}}(t)v_{\mathrm{b}}(t)$ and $P_{\mathrm{e,nl}}(t) = f_{\mathrm{e,nl}}(t)v_{\mathrm{b}}(t)$, for the linear and weakly nonlinear models, respectively.

and absorbed power. Compared to modelling methods, control strategies have a more significant influence on WEC motion and performance. For the case of $R = 20\ \mathrm{m}$, the WEC displacement, restoring force, excitation force, captured power, and absorbed power are shown in Figs. 7(f)-(j), respectively. The WEC natural period is about 9.08 s, which is close to the prevailing wave period ($T_\mathrm{e} = 8.25\ \mathrm{s}$). Thus, difference control strategies, i.e. PC and RC, only slightly affect the WEC dynamics and power absorption. Thus, the deviation between linear and weakly nonlinear modelling methods seems more significant. However, the normalised root-mean-square deviation for the case of $R = 20\ \mathrm{m}$ is still smaller than that for $R = 10\ \mathrm{m}$.

To evaluate WEC motions and performance over a wide range of radius values, the upper boundary is set at 40 m. However, the algebraic solutions to the nonlinear FK and buoyancy forces in Eqs. (24)-(25) assume that the WEC is a point absorber. A large radius may induce some error in the weakly nonlinear hydrodynamic modelling method, and the margin of error is related to the ratio of the sphere diameter to the prevailing wavelength [56]. In addition, the control or PTO parameters in RC and PC, via Eqs. (33)-(34), are selected at the energy period of each sea state, which is taken as a single representative value, showing the panchromatic limitations of RC and PC.

VII. Conclusion

In this study, a semi-submerged heaving sphere is used to investigate the impact of linear and nonlinear hydrodynamic modelling methods on WEC geometric optimisation, and the interplay between the effect of sea states, modelling methods, control strategies and performance criteria on optimal solutions is discussed.

The main findings are: (i) The selection of WSI modelling method can significantly influence the optimised WEC geometry. In this study, the weakly nonlinear hydrodynamic modelling method, considering nonlinear FK and buoyancy forces, generally results in a larger radius than that of the linear method. (ii) The optimised geometry is also sensitive to wave conditions, and an energetic sea state always leads to a larger hull. (iii) Control also plays an important role in WEC geometric optimisation, and the optimised geometry by RC is much smaller than its counterpart by PC, but may lead to unrealistic displacement excursions, particularly with a linear hydrodynamic model. (iv) The selection of an appropriate performance criterion is the most important factor in WEC geometric optimisation, regarding the optimised shape. On the other hand, some performance criteria may be multi-modal or monotonic in the parameter space, requiring extra attention in choosing optimisation algorithms and ranges for the parameter space. (v) In the optimisation loop, WSI modelling naturally has an interdependency with sea states, control strategies and performance criteria and, hence, a co-design framework considering all the aforementioned factors is required.

Ongoing work focuses on validating the effectiveness of the weakly nonlinear modelling method for WEC geometric optimisation by CFD simulation in OpenFOAM, and developing advanced control strategies to handle both nonlinear WEC hydrodynamics and motion constraint.

Acknowledgement

This project has received funding from the European Union's Horizon 2020 research and innovation programme under the Marie Skłodowska-Curie grant agreement No. 841388 and Science Foundation Ireland under Grant No. 12/RC/2302_P2 for the Marine and Renewable Energy Ireland (MaREI) centre. Special thanks owe to Dr. Yerai Pena-Sanchez for his great help in using FOAMM for radiation approximation.

References

[1] B. Holmes and K. Nielsen, "Guidelines for the development & testing of wave energy systems," Ocean Energy Systems, Tech. Rep. OES–IA Document No: T02-2.1, 2010.

[2] J. W. Weber, D. Laird, R. Costello, J. Roberts, D. Bull, A. Babarit, K. Nielsen, C. B. Ferreira, and B. Kennedy, "Cost, time, and risk assessment of different wave energy converter technology development trajectories," in *Proc. European Wave and Tidal Energy Conference*, Cork, Ireland, 2017.

[3] J. Weber, R. Costello, and J. Ringwood, "WEC technology performance levels (TPLs)-metric for successful development of economic WEC technology," in *Proc. European Wave and Tidal Energy Conference*, Aalborg, Denmark, 2013.

[4] J. Hodges, J. Henderson, L. Ruedy, M. Soede, J. Weber, P. Ruiz-Minguela, H. Jeffrey, E. Bannon, M. Holland, R. Maciver, D. Hume, J. Villate, and T. Ramsey, "An international evaluationg and guidance framework for ocean energy technology," Ocean Energy Systems, Tech. Rep., 2021.

[5] B. Guo and J. Ringwood, "A review of wave energy technology from a research and commercial perspective," *IET Renew. Power Gener.*, 2021, in process.

[6] R. Costello, B. Teillant, J. Weber, and J. Ringwood, "Techno-economic optimisation for wave energy converters," in *Proc. International Conference on Ocean Energy*, Dublin, Ireland, 2012, pp. 1–5.

[7] A. De Andres, J. Maillet, J. Hals Todalshaug, P. Möller, D. Bould, and H. Jeffrey, "Techno-economic related metrics for a wave energy converters feasibility assessment," *Sustainability*, vol. 8, no. 11, p. 1109, 2016.

[8] S. A. Sirigu, L. Foglietta, G. Giorgi, M. Bonfanti, G. Cervelli, G. Bracco, and G. Mattiazzo, "Techno-economic optimisation for a wave energy converter via genetic algorithm," *J. Mar. Sci. Eng.*, vol. 8, no. 7, p. 482, 2020.

[9] G. Giorgi, M. Penalba, and J. V. Ringwood, "Nonlinear hydrodynamic models for heaving buoy wave energy converters," in *Proc. Asian Wave and Tidal Energy Conference*, Marina Bay Sands, Singapore, 2016, pp. 1–10.

[10] A. McCabe, G. Aggidis, and M. Widden, "Optimizing the shape of a surge-and-pitch wave energy collector using a genetic algorithm," *Renew. Energy*, vol. 35, no. 12, pp. 2767–2775, 2010.

[11] T. Bódai and N. Srinil, "Performance analysis and optimization of a box-hull wave energy converter concept," *Renew. Energy*, vol. 81, pp. 551–565, 2015.

[12] S. Bozzi, R. Archetti, and G. Passoni, "Wave electricity production in italian offshore: A preliminary investigation," *Renew. Energy*, vol. 62, pp. 407–416, 2014.

[13] L. Wang and J. V. Ringwood, "Geometric optimization of a hinge-barge wave energy converter," in *Proc. European Wave and Tidal Energy Conference*, Naples, Italy, 2019, pp. 1–10.

[14] A. Ulazia, G. Esnaola, P. Serras, and M. Penalba, "On the impact of long-term wave trends on the geometry optimisation of oscillating water column wave energy converters," *Energy*, vol. 206, p. 118146, 2020.

[15] L. Wang and J. V. Ringwood, "Control-informed ballast and geometric optimisation of a three-body hinge-barge wave energy converter using two-layer optimisation," *Renew. Energy*, vol. 171, pp. 1159–1170, 2021.

[16] J. C. Gilloteaux and J. Ringwood, "Control-informed geometric optimisation of wave energy converters," in *Proc. IFAC Conference on Control Applications in Marine Systems*, Rockstock, Germany, 2010, pp. 366–371.

[17] P. B. Garcia-Rosa and J. V. Ringwood, "On the sensitivity of optimal wave energy device geometry to the energy maximizing control system," *IEEE Trans. Sustain. Energy*, vol. 7, no. 1, pp. 419–426, 2016.

[18] A. Garcia-Teruel, D. I. Forehand, and H. Jeffrey, "Metrics for wave energy converter hull geometry optimisation," in *Proc. European Wave and Tidal Energy Conference*, Naples, Italy, 2019, pp. 1–6.

[19] S. A. Sirigu, L. Foglietta, G. Giorgi, M. Bonfanti, G. Cervelli, G. Bracco, and G. Mattiazzo, "Techno-economic optimisation for a wave energy converter via genetic algorithm," *J. Mar. Sci. Eng.*, vol. 8, no. 482, pp. 1–29, 2020.

[20] A. Garcia-Teruel, B. DuPont, and D. I. Forehand, "Hull geometry optimisation of wave energy converters: On the choice of the optimisation algorithm and the geometry definition," *Appl. Energy*, vol. 280, p. 115952, 2020.

[21] A. P. McCabe and G. A. Aggidis, "A preliminary study into optimising the shape of a wave energy collector using a genetic algorithm," in *Proc. International Conference on Sustainable Power Generation and Supply*, Nanjing, China, 2009, pp. 1–7.

[22] A. P. McCabe, "Constrained optimization of the shape of a wave energy collector by genetic algorithm," *Renew. Energy*, vol. 51, pp. 274–284, 2013.

[23] R. P. Gomes, J. C. Henriques, L. M. Gato, and A. F. Falcão, "Hydrodynamic optimization of an axisymmetric floating oscillating water column for wave energy conversion," *Renew. Energy*, vol. 44, pp. 328–339, 2012.

[24] N. Y. Sergiienko, M. Neshat, L. S. P. da Silva, B. Alexander, and M. Wagner, "Design optimisation of a multi-mode wave energy converter," in *Proc. International Conference on Ocean, Offshore and Artic Engineering*, Florida, USA, 2020.

[25] A. Garcia-Teruel and D. Forehand, "A review of geometry optimisation of wave energy converters," *Renew. Sustain. Energy Rev.*, vol. 139, p. 110593, 2021.

[26] A. Babarit, A. Clément, J. Ruer, and C. Tartivel, "SEAREV: A fully integrated wave energy converter," in *Proc. Offshore Wind and other Marine Renewable Energies in Mediterranean and European Seas*, Rome, Italy, 2006, pp. 1–11.

[27] J. Goggins and W. Finnegan, "Shape optimisation of floating wave energy converters for a specified wave energy spectrum," *Renew. Energy*, vol. 71, pp. 208–220, 2014.

[28] S. Zheng, A. Antonini, Y. Zhang, D. Greaves, J. Miles, and G. Iglesias, "Wave power extraction from multiple oscillating water columns along a straight coast," *J. Fluid Mech.*, vol. 878, pp. 445–480, 2019.

[29] C. Windt, J. Davidson, and J. V. Ringwood, "High-fidelity numerical modelling of ocean wave energy systems: A review of computational fluid dynamics-based numerical wave tanks," *Renew. Sustain. Energy Rev.*, vol. 93, pp. 610–630, 2018.

[30] B. Bouali and S. Larbi, "Contribution to the geometry optimization of an oscillating water column wave energy converter," *Energy Procedia*, vol. 36, pp. 565–573, 2013.

[31] J. C. Martins, M. M. Goulart, M. d. N. Gomes, J. A. Souza, L. A. Rocha, L. A. Isoldi, and E. D. dos Santos, "Geometric evaluation of the main operational principle of an overtopping wave energy converter by means of Constructal Design," *Renew. Energy*, vol. 118, pp. 727–741, 2018.

[32] C. W. Hodge, "Pitching paddles, hydraulic PTOs and shallow water waves: The development of a coupled non-linear modelling approach for WEC design," Ph.D. dissertation, University of Edinburgh, 2020.

[33] A. F. Falcão, J. C. Henriques, and J. J. Cândido, "Dynamics and optimization of the OWC spar buoy wave energy converter," *Renew. Energy*, vol. 48, pp. 369–381, 2012.

[34] L. Papillon, R. Costello, and J. V. Ringwood, "Boundary element and integral methods in potential flow theory: A review with a focus on wave energy applications," *J. Ocean Eng. Mar. Energy*, vol. 6, pp. 303–337, 2020.

[35] B. Guo and J. Ringwood, "Geometric optimisation of wave energy conversion devices: A survey," *Appl. Energy*, 2021, in process.

[36] "AMETS Berth B Wave Buoy," http://www.oceanenergyireland.ie/Observation, accessed: 2020-09-10.

[37] K. Hasselmann, T. Barnett, E. Bouws, H. Carlson, D. Cartwright, K. Enke, J. Ewing, H. Gienapp, D. Hasselmann, P. Kruseman *et al.*, "Measurements of wind-wave growth and swell decay during the Joint North Sea Wave Project (JONSWAP)," *Ergänzungsheft 8-12*, 1973.

[38] W. J. Pierson Jr and L. Moskowitz, "A proposed spectral form for fully developed wind seas based on the similarity theory of SA Kitaigorodskii," *J. Geophys. Res.*, vol. 69, no. 24, pp. 5181–5190, 1964.

[39] A. Pecher and J. Peter Kofoed, *Handbook of Ocean Wave Energy*. Springer Nature, 2017.

[40] A. Mérigaud and J. V. Ringwood, "Free-surface time-series generation for wave energy applications," *IEEE J. Oceanic Eng.*, vol. 43, no. 1, pp. 19–35, 2017.

[41] W. Cummins, "The impulse response function and ship motions," *Schiffstechnik*, vol. 9, pp. 101–109, 1962.

[42] T. F. Ogilvie, "Recent progress toward the understanding and prediction of ship motions," in *Proc. Symposium on Naval Hydrodynamics*, Bergen, Norway, 1964, pp. 3–80.

[43] T. Pérez and T. Fossen, "Time-vs. frequency-domain identification of parametric radiation force models for marine structures at zero speed," *Modeling, Identification and Control*, vol. 29, no. 1, pp. 1–19, 2008.

[44] B. Guo, R. Patton, S. Jin, J. Gilbert, and D. Parsons, "Nonlinear modeling and verification of a heaving point absorber for wave energy conversion," *IEEE Trans. Sustain. Energy*, vol. 9, no. 1, pp. 453–461, 2017.

[45] T. Perez and T. Fossen, "A Matlab toolbox for parametric identification of radiation-force models of ships and offshore structures," *Modeling, Identification and Control*, vol. 30, no. 1, pp. 1–15, 2009.

[46] N. Faedo, Y. Peña-Sanchez, and J. V. Ringwood, "Finite-order hydrodynamic model determination for wave energy applications using moment-matching," *Ocean Eng.*, vol. 163, pp. 251–263, 2018.

[47] Y. Pena-Sanchez, N. Faedo, M. Penalba, G. Giorgi, A. Mérigaud, C. Windt, D. G. Violini, L. Wang, and J. V. Ringwood, "Finite-order hydrodynamic approximation by moment-matching (foamm) toolbox for wave energy applications," in *Proc. European Wave and Tidal Energy Conferebce*, Naples, Italy, 2019, pp. 1–9.

[48] Z. Yu and J. Falnes, "State-space modelling of a vertical cylinder in heave," *Appl. Ocean Res.*, vol. 17, no. 5, pp. 265–275, 1995.

[49] B. Guo, R. Patton, and S. Jin, "Identification and validation of excitation force for a heaving point absorber wave energy convertor," in *Proc. European Wave and Tidal Energy Conferebce*, Cork, Ireland, 2017, pp. 1–9.

[50] B. Guo, R. J. Patton, S. Jin, and J. Lan, "Numerical and experimental studies of excitation force approximation for wave energy conversion," *Renew. Energy*, vol. 125, pp. 877–889, 2018.

[51] Y. Peña-Sanchez, C. Windt, J. Davidson, and J. V. Ringwood, "A critical comparison of excitation force estimators for wave-energy devices," *IEEE Trans. Control Syst. Technol.*, pp. 2263–2275, 2019.

[52] A. Merigaud, J.-C. Gilloteaux, and J. V. Ringwood, "A nonlinear extension for linear boundary element methods in wave energy device modelling," in *Proc. International Conference on Offshore Mechanics and Arctic Engineering*, Rio de Janeiro, Brazil, 2012, pp. 1–7.

[53] J. R. Morison, J. W. Johnson, and S. A. Schaaf, "The force exerted by surface waves on piles," *Journal of Petroleum Technology*, vol. 2, no. 05, pp. 149–154, 1950.

[54] G. Giorgi and J. V. Ringwood, "Nonlinear Froude-Krylov and viscous drag representations for wave energy converters in the computation/fidelity continuum," *Ocean Eng.*, vol. 141, pp. 164–175, 2017.

[55] G. Giorgi and J. Ringwood, "Consistency of viscous drag identification tests for wave energy applications," in *Proc. European Wave and Tidal Energy Conference*, no. 643, Cork, Ireland, 2017, pp. 1–8.

[56] G. Giorgi and J. V. Ringwood, "Computationally efficient nonlinear Froude–Krylov force calculations for heaving axisymmetric wave energy point absorbers," *J. Ocean Eng. Mar. Energy*, vol. 3, no. 1, pp. 21–33, 2017.

[57] J. Falnes, *Ocean Waves and Oscillating Systems: Linear Interactions Including Wave-Energy Extraction*. Cambridge University Press, 2002.

[58] P. B. Garcia-Rosa, G. Bacelli, and J. V. Ringwood, "Control-informed geometric optimization of wave energy converters: The impact of device motion and force constraints," *Energies*, vol. 8, no. 12, pp. 13 672–13 687, 2015.

[59] W. Sheng and A. Lewis, "Power takeoff optimization for maximizing energy conversion of wave-activated bodies," *IEEE J. Oceanic Eng.*, vol. 41, no. 3, pp. 529–540, 2016.

[60] B. Teillant, R. Costello, J. Weber, and J. Ringwood, "Productivity and economic assessment of wave energy projects through operational simulations," *Renew. Energy*, vol. 48, pp. 220–230, 2012.

[61] J. Chozas, "International levelised cost of energy for ocean energy technologies," Ocean Energy System, Tech. Rep., 2015.